Fabrication of novel NiO/Ag-CQDs nanocomposites and investigation of effective dye degradation and suppression of bacterial pathogens.

G. Sri balaji *, S. Satheeskumar ,

Centre for Nanoscience and Technology, KS Rangasamy College of Technology, Tiruchengode 637 215, Namakkal (Dt.), Tamil Nadu, India.

Abstract

The photocatalytic and antibacterial activity of nickel oxide and silver-doped carbon quantum dots (NiO/Ag-CQDs) composites was investigated against malachite green dye and pathogenic bacteria such as *Staphylococcus aureus (*gram-positive) and *Escherichia coli* (gram-negative). The nickel oxide and silver-doped carbon quantum dots were prepared through the sonochemical and hydrothermal methods, respectively. The Ag-CQDs were dispersed on the NiO nanoparticles through the reflux method. The synthesized nanomaterials were analyzed using various techniques such as XRD, FTIR, UV-Vis spectrum, PL, and SEM with EDAX. The prepared nanomaterial exhibited 30.12 nm and 1.9 nm particle size for the NiO NPs and Ag-CQDs, and the equally distributed silver-doped carbon quantum dots throughout the surface of the NiO NPs were revealed through the SEM representations. From UV-vis spectra, NiO/Ag-CQDs exhibited an efficient photocatalytic degradation efficiency of 92 % for the MG dye in an aqueous medium within 135 min. TheNiO/Ag-CQDs composite exhibited antibacterial activity with 20.5 mm and 19.8 mm of the zone of inhibition for the gram-positive and gram-negative pathogenic bacteria, respectively. The observed results revealed that the prepared nanocomposite could be a potential composite for multifunctional application.

Keywords - Silver doped carbon quantum dots, Nickel oxide nanoparticle, Hydrothermal, Photocatalytic activity, Antibacterial activity,and Sonochemical synthesis.

1. Introduction

The environment is increasingly concerned about releasing industrial leachate into untreated rivers and lakes. Considering the damage it does to aquatic and human health, The ecology is seriously threatened by hazardous pollutants present in effluents, such as dyes and dangerous bacterial pathogens. To create a healthier and cleaner environment, developing efficient and long-lasting materials for bacterial growth suppression and dye degradation is crucial.

Since dyes are released into freshwater resources, they substantially damage the environment since they are utilized in many industries, such as lambskin, polymers, and textiles. Dyes can be either artificial or natural. Malachite green is an ectoparasiticide and fungicide that is commonly used in the world's fish

farming industry [1]. Although widely used, MG is still a contentious substance because of its carcinogenic, mutagenic, teratogenic, and respiratory toxicity-causing characteristics [2]. On the other hand, bacterial pathogens such as gram-positive *Staphylococcus aureus* and gram-negative *Escherichia coli* are to blame for many diseases in both people and animals. More than a century later, *Staphylococcus aureus* is still a lethal and adaptable pathogen in humans. Although there has been no change in overall mortality, staphylococcal infection rates have steadily increased in both the community and hospitals [3]. Moreover, several extremely virulent E. coli clones possess evolved unique pathogenicity features, enhancing their adaptability to various settings and permitting them to transmit a range of illnesses. These pathogenic traits are frequently conserved on genes encoding proteins that may have formerly been mobile but have since changed to become "frozen" inside the genome or on genetic elements that may be linked with gene mutations from various strains to produce new virulence factors. Only strong combinations of virulence factors have been able to identify different "pathotypes" of E. coli that could infect humans [4]. Nanomaterials have recently sparked attention across a range of sectors because of their unique physical-chemical characteristics and possible uses. Both metal and metal oxide nanoparticles have different surface, optical, thermodynamic, and physical properties from their native bulk components, in addition to having different physical and chemical properties. Reducing, oxidizing, or precipitating agents are employed to create nanoparticles for making metal and metal oxide nanoparticles [5]. Many types of nanoparticles and their derivatives have generated much interest because of their conceivable antibacterial characteristics. Several metal nanoparticles, such as Ag_2O, TiO_2, Si, CuO, ZnO, and MgO, have antibacterial characteristics. Many bacterial species were demonstrated to be suppressed by metal nanoparticles in vitro tests [6]. Metal and metal oxide nanoparticles are one of the most researched nanomaterials for fighting multidrug-resistant bacteria [7]. Owing to their simple manufacture, nontoxicity, superior biocompatibility, and simplicity of surface modification, CQDs have a unique family of metal-free fluorescent nanoparticles that mimic semiconductor quantum dots, attracting researchers' attention. They have several applications in various fields, including bacterial imaging and sensor-based, drug and gene transport, catalysis, and signaling [8]. Past surveys indicate that remarkable electron donors and electron acceptors may be made from hyper-photosensitive carbon-based quantum dots, such as those made of carbon (CQDs). Nonetheless, Ni is one of the good materials, and NiO is the focus of our attention. Due to its good thermal stability, low price, naturally plentiful supply, relatively high rate capability, and environmental stewardship [9]. Several antimicrobial and biophysical investigations were used to investigate the antibacterial activity of NiO NP. According to previous research, as compared to gram-negative bacteria, gram-positive bacteria are more sensitive to the antibacterial effects of NiO NP [10]. Silver has long been used in human treatment as an antimicrobial. It was developed for use in surgical appliances, bone prostheses, cardiac implants, purification of water, wound care, and orthopaedic multiple surgeries [11]. And silver possesses a surface

plasmon resonance feature. That happens when it shows a significant oscillation at a particular light wavelength. It has high photosensitivity.

In this paper, we use a simple and affordable reflux method to create NiO/Ag-CQDs composite. Every method utilized to make the nanomaterials was safe for the environment, and many techniques were used to describe the characteristics of the synthesized nanomaterials. Here, the disc diffusion method assessed the antibacterial activity against *Staphylococcus aureus* and *Escherichia coli*, and their measurement of antibacterial growth inhibition was shown by a bar graph. The photocatalytic degradation of the created nanocomposites was looked into while utilizing MG as a model pollutant. UV-Vis spectroscopy was used to assess the malachite green dye's ability to degrade.

2. Experimental section

2.1. Materials

All chemicals used were of analytical quality, acquired from Loba Chemie, (India). The primary components were Ethylenediamine ($C_2H_4(NH_2)_2$), Sodium hydroxide (NaOH), Silver nitrate ($AgNO_3$), and Nickel nitrate ($Ni(NO_3)_2$). All tests and investigations employed deionized water as their synthesizing medium.

2.2. Synthesis of Nickel Oxide

The primary beaker consists of 5.481g of nickel nitrate dissolved in 300 ml of deionized water, and the other beaker consists of 0.799g of sodium hydroxide dissolved in 100 ml of deionized water. With the aid of a burette, the NaOH is added dropwise at a slow speed to the primary beaker. The primary beaker containing the nickel nitrate was placed in a magnetic stirrer and swirled continuously at a speed of 250 RPM. Until the pH of the primary beaker solution became base, the reduction agent NaOH was continuously added. After the pH reaches 10, the stirrer is stopped, Then the mixture was sonicated for 1 hrs to dissociate the nickel nitrate precursors solution. After the sonication process, the mixture solution was kept againg for 24 hrs and take the complete reduction reaction.The mixture was thereafter dried for eight hours in a hot air oven at 60 °C. To get the high crystalline natural NiO, the dried sample was calcined at 400 °C for 4 hours.

2.3. Synthesis of silver-doped carbon quantum dot

To make silver-doped carbon quantum dots 3 ml of ethylenediamine was added to 90 ml of H_2O, along with 0.3 g of silver nitrate, and the mixture was agitated using a magnetic stirrer at a speed of 1000 RPM. The entire solution was transferred to the Teflon-lined autoclave, which was placed in a hot air oven and heated for 6 hours at 180℃. The resulting solution was allowed to cool to room temperature. Finally, a

0.22µm membrane was used to filter the resultant solution internally to eliminate contaminants and bulk particles. The prepared high purity of silver-doped carbon quantum dots were collected and shown in Fig. 1.

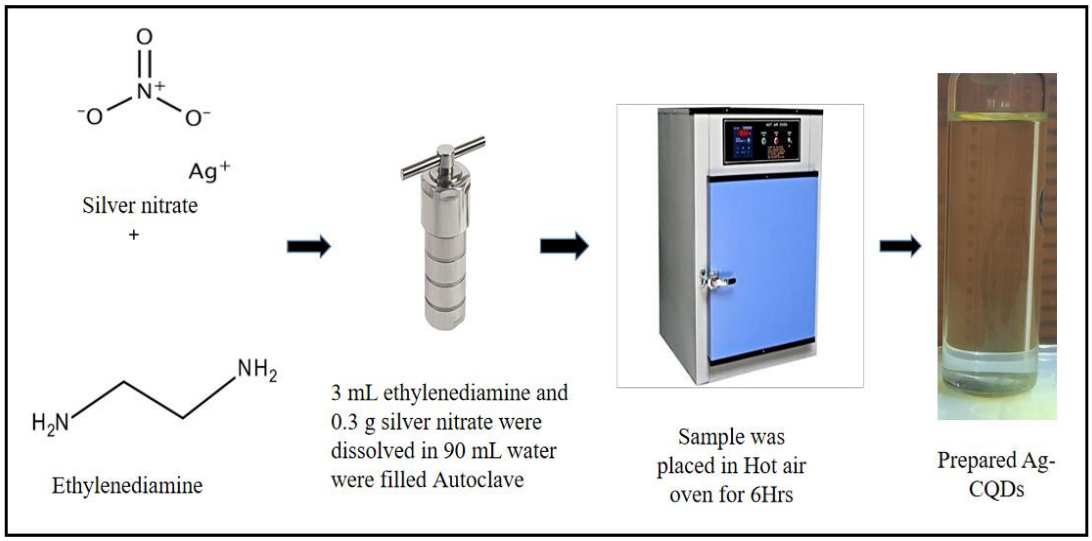

Fig. 1. Schematical representation of preparation silver-doped carbon quantum dot.

2.4. Synthesis of Nickel Oxide and silver-doped carbon quantum dot composite

A nanocomposite is created by dissolving 100 ml of deionized water with 100 mg of synthesized nickel oxide nanoparticles and 5 ml of Ag-CQDs. The combination underwent ultrasonication for one hour. Then it was poured into a flask with a circular bottom that was attached to the condenser. 80 °C for three hours of condensation Finally, the nanocomposite solution was heated enough to make it a dry powder.

2.5. Characterization techniques

The behavior of nanoparticles it's depends on their physicochemical characteristics. Thus, NiO/Ag-CQDs characterization is crucial to assess the functional characteristics of the created nanomaterials. Numerous analytical methods are used to characterize the samples, such as the Agilent Cary 8454 UV-Visible spectroscopy from Singapore, and the X-ray diffractometry (XRD) from PANalytical in Almelo, the Netherlands, The samples were scanned at a rate of $10s^{-1}$ in the frequency range of 5.0-90.00° angle (2θ) using Cu-Kα as the source of radiation (k = 1.54060 Å) at a voltage of 40 kV (30 mA). the Fourier transform infrared spectroscopy (FTIR) from PerkinElmer in the United States, the study investigated functional groups of all prepared material in the natural environment using KBr material as the background. Photoluminescence spectroscopy (PL), Scanning electron microscopy (SEM), and (EDX) Energy-dispersive X-ray spectroscopy, were used to look at the shape, surface characteristics, and chemical makeup of produced nanomaterials.

2.6. Photocatalytic degradation activity procedure

We measured the effectiveness by the breakdown of malachite green to gauge the ultraviolet light catalytic efficacy of the newly synthesized nanomaterials. Malachite green dye (C23H25ClN2) was combined with produced NiO/Ag-CQDs composite materials (100 mg) with 100 ml of deionized water (diH_2O). After adding the nanocomposite, the initial dye concentration is determined using the UV-Vis spectrum. To test if the malachite green dye breaks down on its own due to the charge carriers from outside light sources, a 100 ml solution is left in the dark. The deterioration was then determined by having the beaker exposed to UV light. Frequently, a tiny sample of the liquid was obtained, and the sample's intensity was calculated using a UV-Vis spectrum. Moreover, ten replicate tests were used to investigate the catalyst's rate capability.

$$Efficiency(\%) = \left(\frac{C_0 - C_e}{C_0} \right) \times 100 \quad (1)$$

where C_e and C_o stand for the dye's first and last percentages before and following photo-irradiation, respectively. E% in this equation represents the percentage of dye photocatalyst degradation [12].

2.7. Antimicrobial study

2.7.1. Collection and culture preparation

The anti-bacterial performance of the NiO/Ag-CQDs nanocomposite was evaluated using the Kirby-Bauer disc diffusion susceptibility test. Testing was done on gram-negative *Escherichia coli* and gram-positive *Staphylococcus aureus* bacterial strains to determine the nanocomposite's antibacterial effectiveness. The National Chemical Laboratory in Pune, India provided the Staphylococcus aureus (ATCC 6538P) and Escherichia coli (ATCC 9677) bacterial cultures that were utilized to discover CSG scaffolds. During earlier research, nutritious agar medium (M001, HiMedia, Bombay, India) bacterial cultures were stored for subculturing at 4°C in a freezer.

2.7.2. Bacterial growth inhibition test

In a conical flash, 3g nutrient agar was dissolved in 250 ml water. which were sealed with cotton plunge and then it was placed in an autoclave together petri dish also placed which were heated for 30 minutes. 20 to 30 ml of agar were added to each disc after 10 minutes, and once they had cooled to room temperature, the agar medium solidified. Cut a few little circles for the porous nanocomposite zone. The swabs are used to transmit each bacterial in each disc. It was gently swiped across the entire area of solid nutrient agar to disseminate the bacteria after being dipped into the cultivated bacteria, by following the placement of the standard cotton disc. In 5 ml of distilled water, 2 mg of the prepared nanocomposite was dissolved. 5µL, 10µL, and 15µL of the produced nanocomposite were pipetted into the porous Petri dish

using a micropipette. The laminar airflow chamber served as the setting for this exchange. The plates were inverted and put in an incubator at 37℃ for 24 hours. Following the overnight incubation, the antibacterial agent sample is surrounded by a clear zone known as the inhibition zone, which is seen and quantified.

3. Results and discussion

3.1. Optical absorption and energy band gap of prepared nanoparticles

UV-Vis and photoluminescence spectroscopy were used to examine the produced nanomaterial's optical characteristics. Fig. 2 illustrates the prepared nickel oxide test results revealed a λmax peak at 308 nm [13], along with a slight shift absorbed in the visible area, indicating that the prepared NiO nanoparticles have grown in size due to a narrowing of the band gap. And the synthesized Ag-doped carbon quantum dot showed a λmax absorption peak at 300 nm [14], finally, the reflux approach prepared nanocomposite exhibits a significant absorption peak at 300nm. Fig. 3 shows the prepared Ag-CQDs emits fluoresces vivid blue when exposed to 365 nm of the UV lamp.

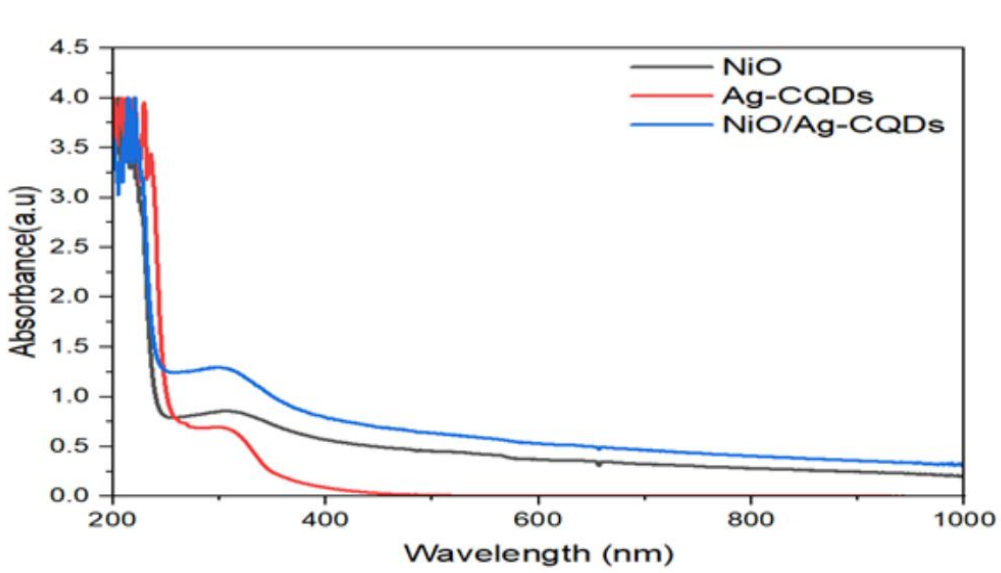

Fig. 2.Optical properties of NiO NPs, Ag-CQDs, and NiO/Ag-CQDs under UV–Vis spectrum

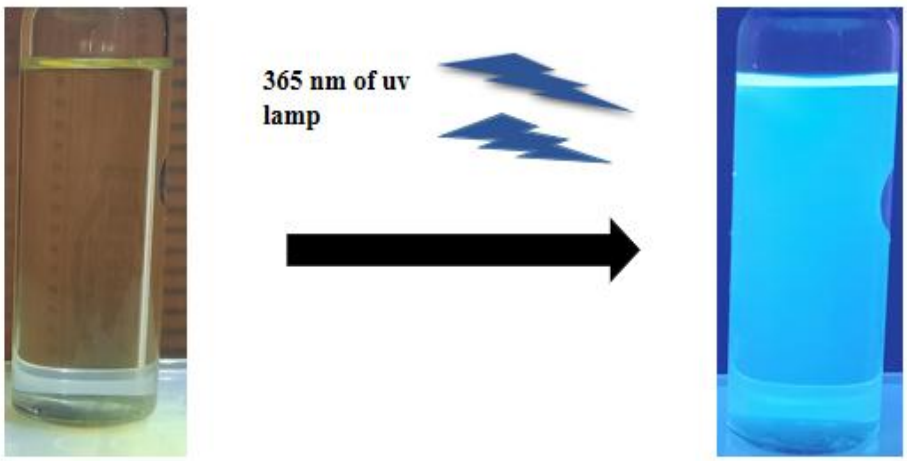

Fig. 3. Under UV irradiation, a produced Ag-Carbon quantum dot generates blue fluorescence.

The following equation describes the relationship between the absorption coefficient (α) and the semiconductor's optical bandgap (E_g).

$$\alpha h\nu = C\left(h\nu - E_g\right)^x \tag{2}$$

Here, C is constant, the absorption coefficient is denoted by α, the photon energy is denoted by ħυ, and the x value is denoted by 2 or 1/2 depending on whether the transition is direct or indirect [15]. The development of the indirect gap selection rule with the size is among the most fascinating and ongoing subjects in semiconducting nanostructured photophysics [16]. Employing the tauc relation equation the synthesized silver doped carbon quantum dots and nickel oxide had band gaps of 2.47eV and 3.77eV, respectively. The stated E_g levels for NiO range from 3.6 to 4.0 eV [17]. The E_g of a semiconductor nickel oxide typically lies between the metal d states in the E_c and the O 2p levels in the E_v. It is commonly known that the maximum E_v state for nickel oxide comes from the O 2p states, whereas the least E_c state comes from the Ni 3d states [18].

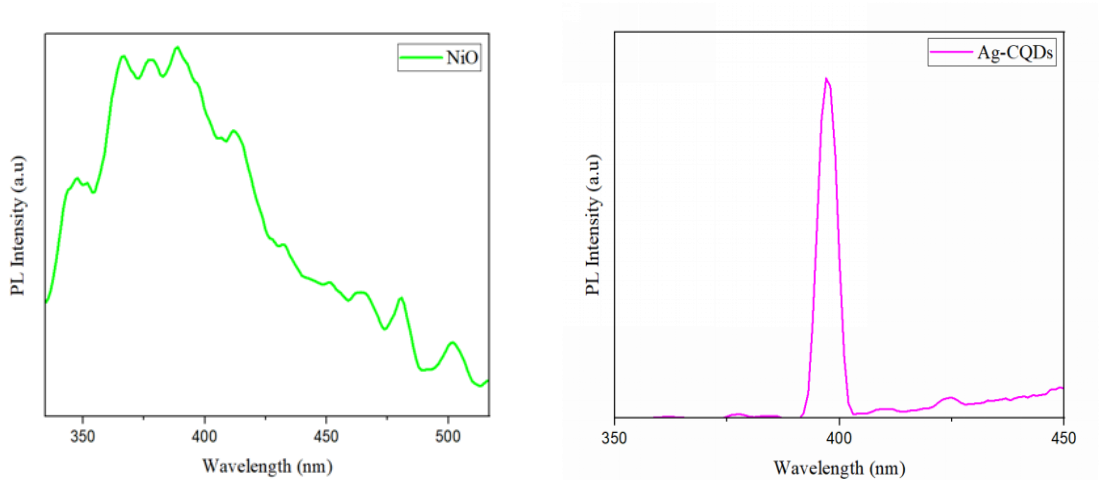

Fig. 4. Emission of prepared nanomaterials investigated using photoluminescence spectrum.

Deep-level defect-related 380-700nm visible emission and (NBE) UV emission are two subgroups of PL that are used to study the excitation and recombination of electrons [19]. The emission behavior of a carbon quantum dot typically occurs below the visible range and is dependent on the activation of an electron in the valence band. As shows in Fig. 4, the maximum emission was at 395 nm for Ag-CQDs. Between 340 and 510 nm, NiO photoluminescence emission spectra were recorded [20].

An electron can be promoted from the E_v to the E_c as a result of a photon being absorbed by the nanomaterials. The ħυ must be equal to or higher than the energy gap between the E_v and E_c to permit this transformation. The consequence is the formation of the exciton, which is an electron-hole pair [21]. Thevisible NiO emission is caused by an electron going via radiative recombination, which fills the oxygen's vacant positions with a photogenerated hole. Nanomaterials' electron transport characteristics are

also greatly influenced by their size. The amount of energy needed to add additional charges to a stretched crystal remains constant [22].

3.2. Structural and functional characteristics of prepared nickel oxide and Ag-doped carbon quantum dot nanoparticles.

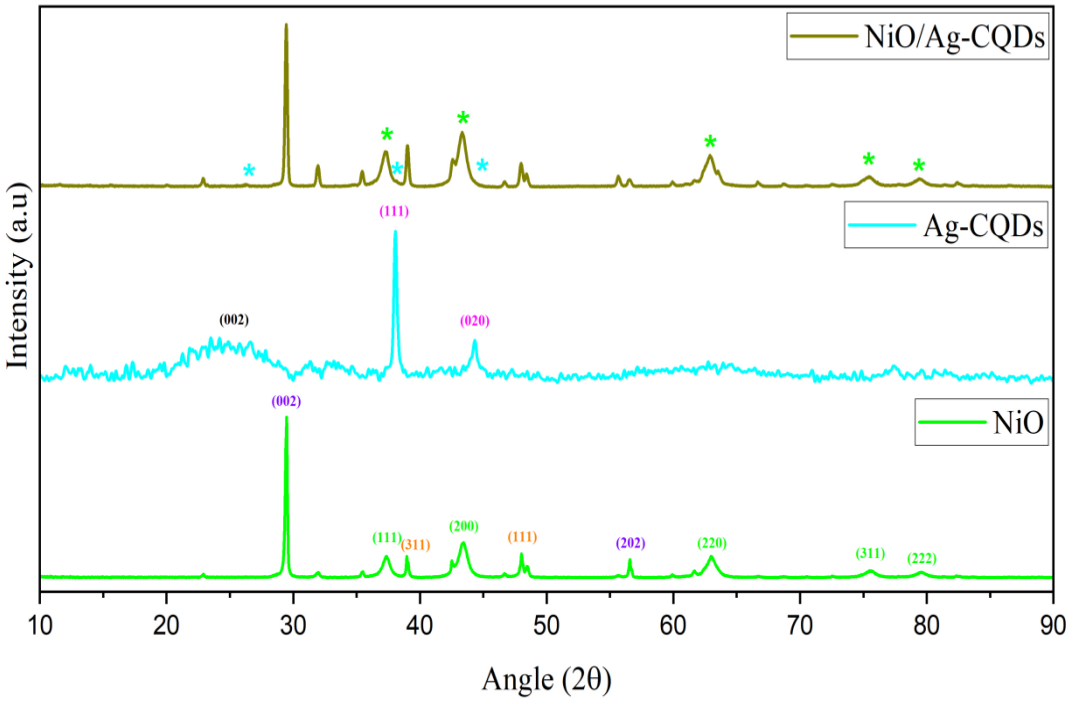

Fig. 5. XRD pattern of prepared nanomaterials.

Fig. 5. Illustrates the XRD patterns of synthesized NiO NPs, Ag-CQDs, and composite. It works by shining incident X-rays on a material, which scatters the light at a predetermined angle of 2θ and then absorbs the intensity of the radiation. The powdered nanoparticle sample's X-ray diffraction pattern clearly distinguishes peaks of 37·34°, 43·34°, 63·12°, 75·62°, and 79·54° are associated with different diffracting planes [111], [200], [220], [311], and [222] about cubic NiO crystallites. The Debye-Scherrer method is used to determine the size of crystals (D). It is used.

$$D = \frac{0.9\lambda}{\beta Cos\ \theta} \qquad (3)$$

The K, also known as the Scherer's constant (K=0.94), θ is Bragg's angle, β is the full width at half max (FWHM) of the peak intensity and λ is the X-ray wavelength (1.54178Å) [23]. The cubic phase of NiO (JCPDS Card 073-1519) with a lattice constant of 4.1700Å was formed, cubic structured phase (a = b = c = 4.170Å & α = β = γ = 90°) and the space-group Fm-3m (225) can be identified from the observed XRD patterns of produced NiO-NPs. The additional peaks designated as Ni_2O_3 that were seen at angles (2θ) of 29.46° and 56.55° correspond to [002] and [202] phases of crystal respectively. Moreover, there are two

additional peaks for nickel that are related to the crystal phases of [311] and [111] at peaks of 38.95° and 48.04°.

The micrograph additionally shows the crystallite aggregation. The nanoscale of the crystalline particles may be the cause of the agglomeration. Since the outermost energy of the tiny particles is high, they combine to reduce their external energy throughout crystal formation [24]. Also, the [002] diffraction peak at 26.63° is strongly related to carbon, despite two high-intensity peaks for [111] and [020] at 38.06° and 44.33°, respectively, indicating the presence of silver. The XRD analysis of the composite made using the reflux method revealed three distinct peaks, a small diffraction peak at 26.6°, which denotes the presence of amorphous carbon, a sharp peak at 38.9°, which is slightly increased over nickel oxide and denotes the presence of Ag and a second silver peak at 44.33 °, which is overlapped in NiO.

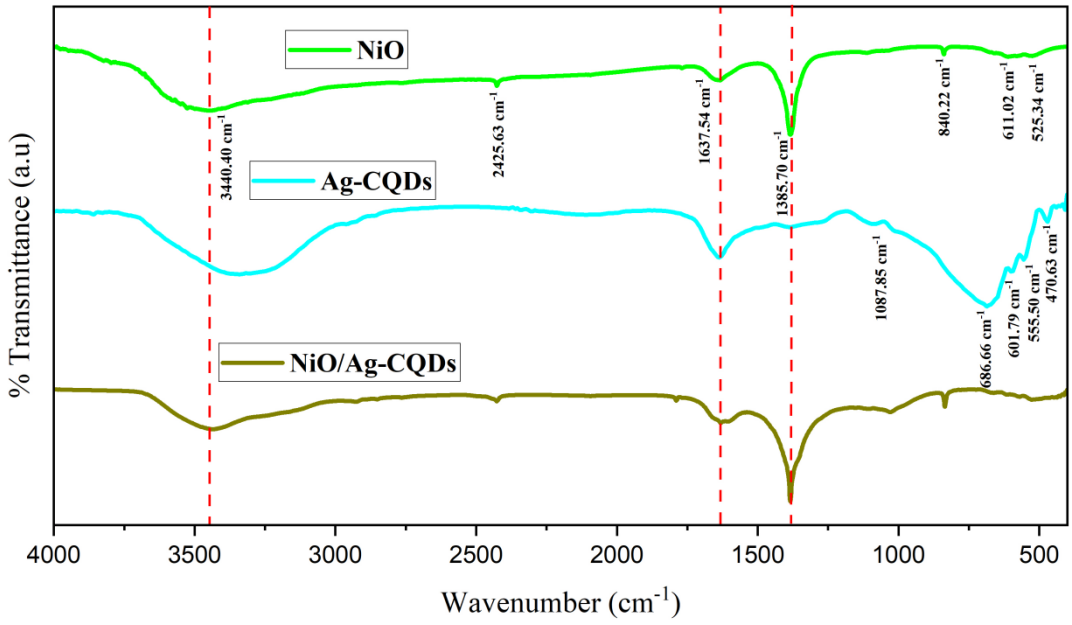

Fig. 6. FT-IR spectrum of NiO nanoparticles, Ag-CQDs, and nanocomposite.

Fig.6 Shows the FT-IR spectrum was utilized to identify the functional group in composite, silver-doped carbon quantum dots and produced nickel oxide. Here, the peak at 3400-3300, 1630-1635, and 1385-1380 cm^{-1}, which are all absorption bands that respect strong O-H stretching, stretching vibrations of the C-C group, and medium C-H bending, is slightly comparable in all synthesized nanomaterials. The NiO FT-IR spectra revealed absorption bands at 2425.63, and 840.22 cm^{-1}, which correspond to medium O=C=O stretching and C=C bending, respectively, and the favourite band of below 800 cm^{-1}, which denotes internal metal vibration. The peak for nickel oxide's stretching vibration is at 611.02 [25], while its bending vibration is at 525.34 cm^{-1}, respectively [26].

After lyophilizing the Ag-CQDs solutions, FT-IR analysis was carried out. The functional groups with mild C-N stretching amine, strong C=C bending, and strong C-O vibration, respectively, it has been demonstrated that it is brought on by moisture-absorbing water molecules, are represented by the

absorption bands at 1087.85, 686.66, and 470.63 cm^{-1}, respectively. The results suggest that Ag-CQDs top layer contains functional groups like oxygen and many others. The NiO/Ag-CQDs composites FT-IR peaks display an absorption band at 2425.07, 1790.35, 1032.67, and 840.36 cm^{-1} that respected to exhibits strong O=C=O stretching, strong C=O stretching, C-N stretching, and medium C=C bending. These completely absorbed bands demonstrate the composites good bond.

3.3. Particle surface morphology and elemental analysis.

Fig.7 Shows the created silver-doped carbon quantum dot as well as the nanostructure and morphology of the nanocomposite site are examined using scanning electron microscopy, which preserves the picture of the nanoparticle. quantum confinement occurs as particle size becomes the same or smaller than the r_{Bohr} radius, the average free route length of electrons, or the electrons charging Coulombic activity. As a general rule, quantum size effects start to show up in materials when the crystallite size drops below 10 nm [27].

Validates the size and form of the particles in the Ag-CQDs. The majority of the Ag-CQDs are spherical and as-prepared size distribution of around 1.97 nm. The quantum dot's diameter and form define its discrete ħυ levels. As an electron relaxes from an excited state to a lower energy state in a 1-2 nm quantum dot, the energy levels are such that the electron produces a photon of blue light. Moreover, the prepared nanocomposite's optical picture demonstrates shows equally distributed the silver-doped carbon quantum dots are throughout the nickel oxide. Moreover, the following picture displays the manufactured nickel oxide stacked layer morphology. The prepared nickel oxide has an average size of around 30.98 nm. The non-stoichiometric makeup of the nickel oxide particles is to blame for the little shifting of the lattice angle [28].Fig. 8 Shows the element mapping performed using energy-dispersive X-ray spectroscopy (EDS) demonstrates the prevalence of the element in Ag-CQDS. Here, the Ag-CQDs display the prepared QDs does not contain any other impurity.

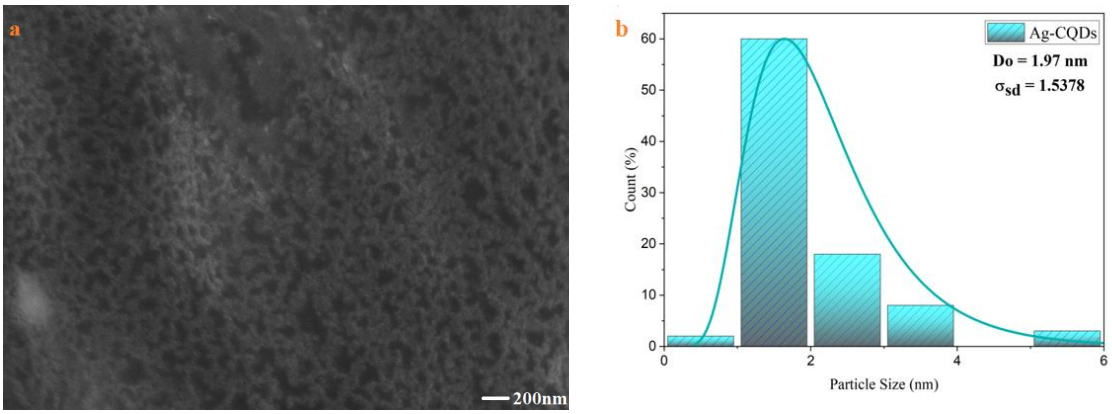

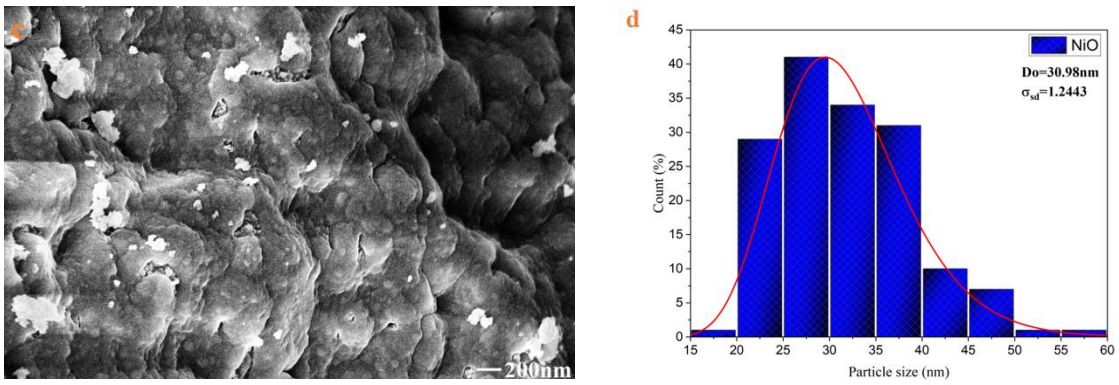

Fig. 7. FESEM picture and computed histogram of particle size of Ag-CQDs (a & b), NiO/Ag-CQDs (c), and NiO (d)

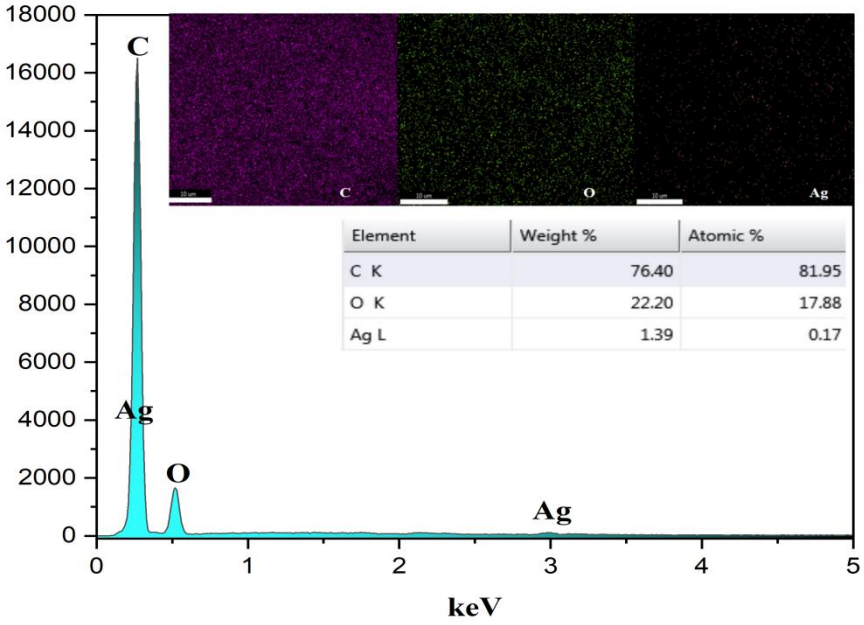

Fig. 8. Elemental composition of prepared Ag-CQDs.

3.4. Photocatalytic activity of NiO/Ag-CQDs

Under the influence of UV light, the photocatalytic performance of nickel oxide and silver-doped carbon quantum dot composites were examined for the degradation of malachite green solution. Here, produced nanocomposites at a 1 mg/ml concentration were added to a 100 ml solution of malachite green. These aqueous suspensions were stirred for 30 minutes in the dark to achieve the equilibrium between absorption and desorption, and then the aqueous solution was transferred to ultraviolet light for photocatalytic activity, every 15 minutes, 2 ml of the aqueous solution was collected to conduct photodegradation assessments under the influence of UV-Vis spectrum. The Malachite green concentrations were identified using a UV-Visible spectrophotometer, with the maximum peak absorbed at 619 nm.

Fig.9. Demonstrates the effectiveness of breaking down malachite green dye by nickel oxide, silver-doped carbon quantum dots, and nanocomposites. During 75 minutes of ultraviolet light exposure. Our findings show that higher degradation performance is optimum for composites. Ag-CQDs were added to nickel oxide to increase their photocatalytic activity.

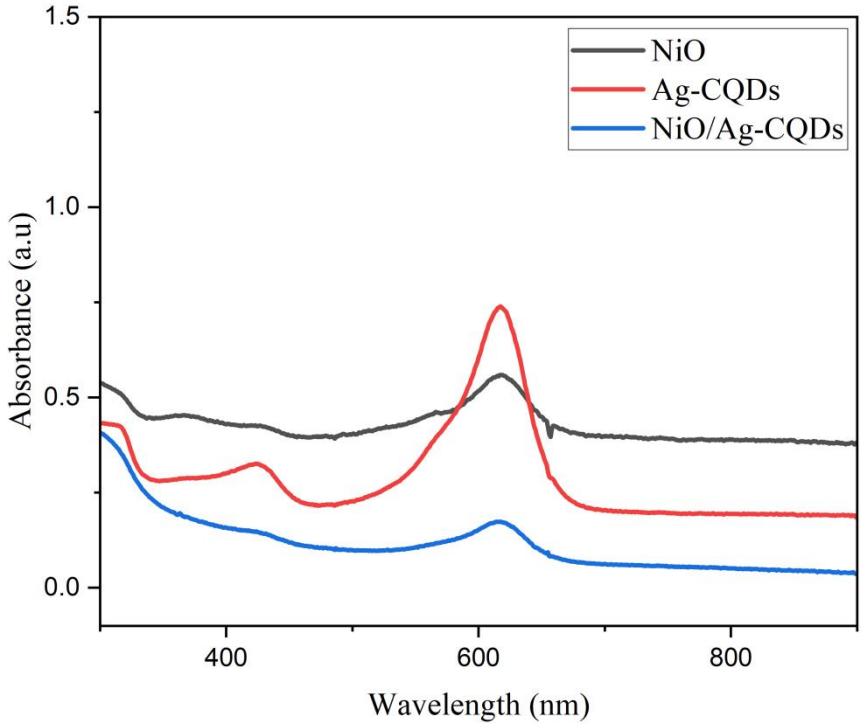

Fig. 9. The photocatalytic performance of prepared nanomaterials in 75 minutes.

The malachite green dye color significantly faded within the first 15 minutes of exposure, and the decolorization rate increased to 37.6% over the subsequent 15 minutes of reaction. After fifteen minutes, the rate of decline accelerated more slowly and virtually linearly. Using the UV spectrum, the intensity changes were measured which are shown in Fig.10. The dye ultimately lost its color after 135 minutes of exposure to UV irradiation, even in a combination of low-concentration Ag-doped carbon quantum dots. By preventing charge recombination, the catalytic capacity of NiO/Ag-CQDs is attributed to photogenerated electron-hole pairs.

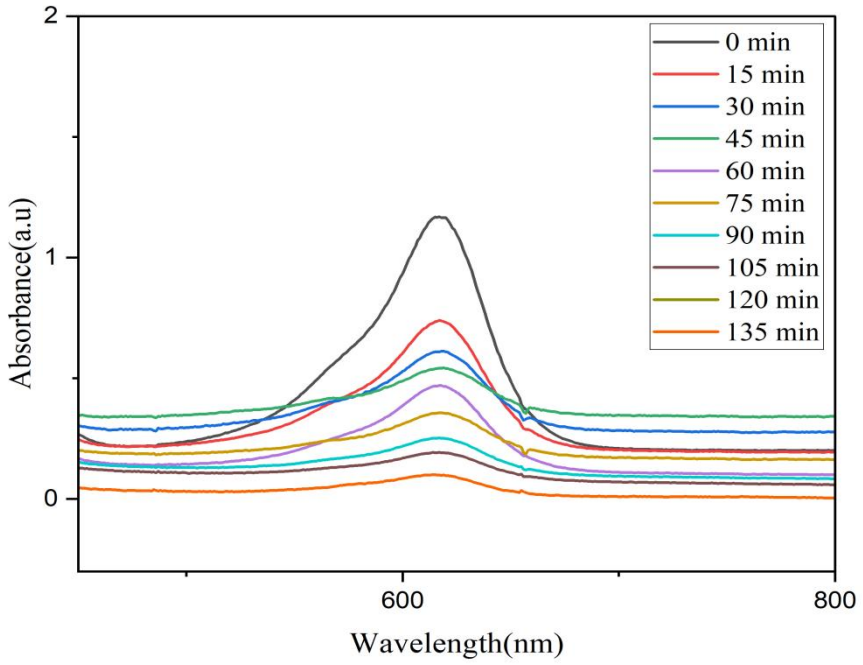

Fig. 10. Photocatalytic performance against malachite green dye.

The electron-hole produced by light is thought to be the catalyst for Ag-CQDs/ NiO's catalytic activity. Fig. 11 Shows a mechanism of significant decomposition and detoxification that occur in the composite when the light is irritated on it. An electron is freed and goes from the E_v to the E_c when light energy is radiated on the nanocomposite, specifically on nickel oxide, by the electron's moment, which creates a hole behind. By preventing charge recombination from producing photosensitive sites, the liberated electron transfers to fill the hole of Ag-CQDs photogenerated electron-hole pairs. The photogenerated charge carriers are thermodynamically prone to join due to Coulombic attraction. Hence, preserving active charge carriers while also preventing their recombination is the best course of action [29].

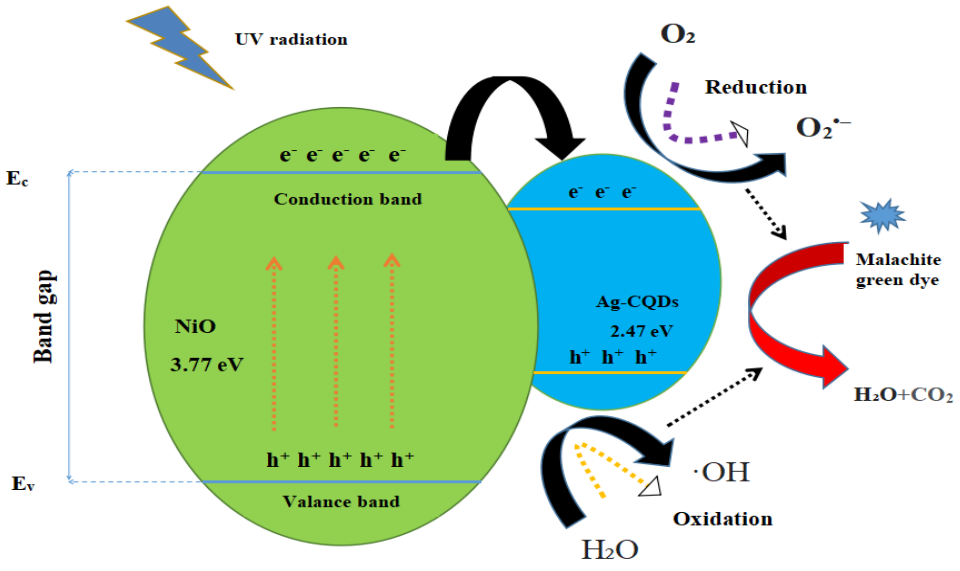

Fig. 11. Degradation mechanism of NiO/Ag-CQDs against malachite green dye under UV irradiation.

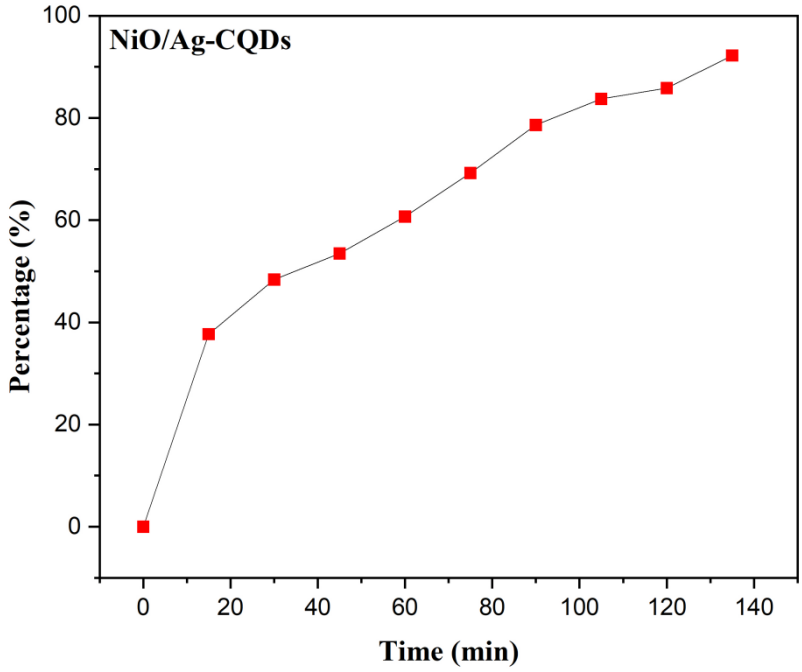

Fig. 12. Percentage of malachite green dye Degradation by NiO/Ag-CQDs

As a result, the oxygen was struck by the expelled electron, turning it into a super oxide anion ($O_2^{\cdot-}$) as a by-product, the composite surface became positively charged. Hence, it takes an electron from the H_2O to fill the hole that exists. After losing one electron, the water turns into a hydroxy radical (·OH). As a result, the produced $O_2^{\cdot-}$ and ·OH were cracked and broke down the malachite green dye. The mentioned factors cause a rise in photogenerated oxidation and ·OH, which improves the degrading efficiency quickly. Correspondingly, while utilizing 1 mg/ml under UV light irritation for 135 minutes, Fig .12 shows the degradation rate might reach 92%.

3.5. Pseudo-first-order kinetic studies for dye degradation

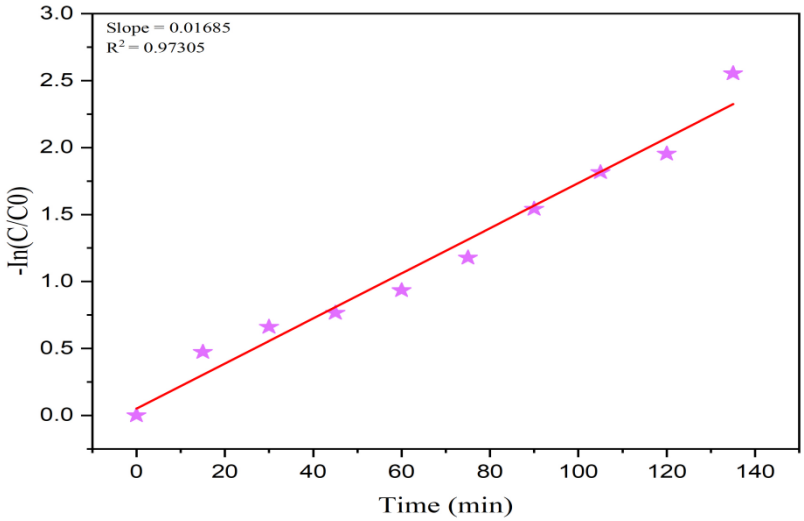

Fig. 13. -In(C/C0) curve of NiO/Ag-CQDs.

As illustrated inFig. 13, Pseudo first order decomposition kinetic processes are used to describe the photocatalytic degradation of produced NiO/Ag-CQDs against malachite green dyes. A equation is used to explore the kinetics of pseudo-first-order deterioration.

$$- In \frac{C_0}{C} = Kt \quad (4)$$

As Malachite green is exposed to radiation, its concentration rises to a new level called C_t. K is the apparent rate constant, initial concentration is MG dye is C_0 and t is the exposure duration [30]. The hypothesis viability is shown by the crossline confirmation of the origin and its 0.97 adjustment coefficient. Hence the rate of a reaction constants for the composite were determined from the slope of the yielding results using linear regression, and they were found to be 0.01685 min^{-1} for NiO/Ag-CQDs.

3.6. Antibacterial activity of NiO/Ag-CQDs

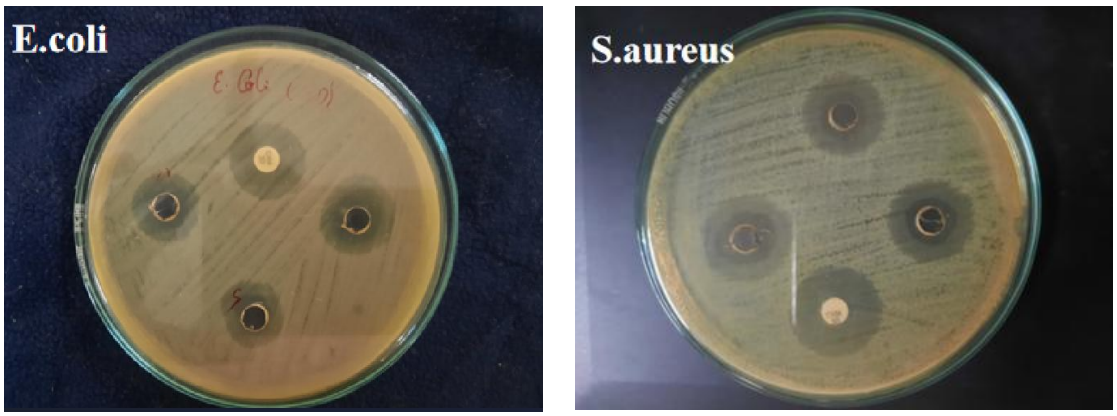

Fig. 14. Antibacterial activity of NiO/Ag-CQDs ability to inhibit the growth of E. coli and S. aureus bacteria

Fig.14. Illustrates an experiment using the synthesized NiO/Ag-CQDs. The samples show excellent antibacterial action versus Gram-negative bacteria *Escherichia coli* and gram-positive bacteria Bacterial *Staphylococcus* aureus. In contrast to composites, the inhibition zone diameter is displayed. Nanocomposites can kill bacteria by generating reactive oxygen compounds like $O_2^{\cdot-}$ and hydrogen peroxide anions (H_2O_2) that interact with the cell wall of bacteria and harm the cell membrane, restricting further pathogenic bacteria growth and causing internal cellular parts to leak out, eventually contributing to bacterial death [31].

The accidental production of $O_2^{\cdot-}$ and H_2O_2 occurs in the cytoplasm predominantly as a result of O_2 coming into contact with different redox enzymes which contain solvent-exposed flavins [32]. The generation of ROS, rupture, and penetration of the bacterial cell membrane and wall, development of oxidative stress with DNA/RNA damage, modification or suppression of key cell proliferation, and

induction of cell stress to proteins and other intracellular macromolecules [33]. Because of their positive charge, nickel oxides can enhance the adherence of negatively charged bacteria to surfaces [34].

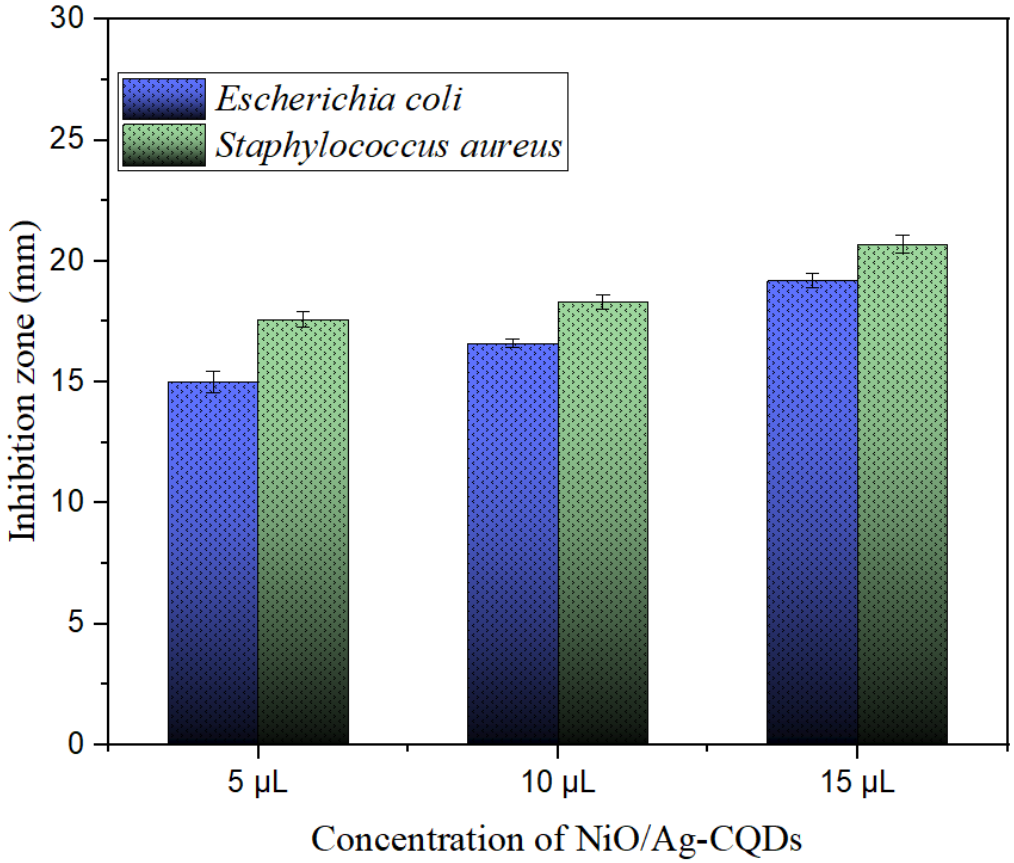

Fig.15 Growth inhibition assay E. coli and S. aureus.

Table.1

Zone of Inhibitions

Inhibition zone			
Dish/Volume	5µl	10µl	15µl
Escherichia coli	15 ± 0.45	16.6 ± 0.17	19.2 ± 0.28
Staphylococcus aureus	17.6 ± 0.31	18.3 ± 0.29	20.7 ± 0.38

Fig. 15 shows the zone of inhibition, Gram staining is a way to differentiate between the two kinds of bacteria. Due to the impenetrability of the cell wall, gram-negative pathogens are much more susceptible to antibodies. Table. 1 shows that opposed to *Escherichia coli*, *Staphylococcus aureus* exhibits a significant zone of inhibition here. Because of the electrostatic interaction of nanocomposite to the cell wall of bacteria, disruption of biological membranes, modification of ventilatory supply line and many permeability-dependent responses, generation of free ROS, promotion of electrostatic interaction between both the positive charge nanomaterials and negative-charged bacteria cells, and subsequent breakdown of bacterial structural proteins [35]. The produced nanocomposite exhibits a robust inhibition zone against both gram-

positive and gram-negative bacteria, while gram-positive bacteria exhibit a significantly greater inhibitory growth. By creating oxidative stress from the nanocomposite, it kills bacteria.

4. Conclusion

In conclusion, the synthesized a stacked layer of nickel oxide utilizing the sonochemical method and a simple hydrothermal manufacturing approach to manufacture exceptionally blue fluorescence silver doped carbon quantum dot species. The NiO/Ag-CQDs composite offers a number of enhancements, including more catalytic active sites and improved photocatalytic reaction activity. Because of using Reflux condensation equally dispersed Ag-CQDs formed on stacked layer nickel oxide, which improves the reactivity of the specimen with ·OH and $O_2^{\cdot-}$. As a result, in 135 minutes of UV irradiation, an effective photocatalytic process of malachite green dye degradation was achieved at 92%.The antibacterial activity of prepared NiO/Ag-CQDs nanocomposite shows the higher zone of inhibition, comparatively*Staphylococcus aureus*, a gram positive bacteria, has a greater zone of inhibitions than *Escherichia coli,* a gramnegative bacteria, according to the antibacterial examination. Hence, the obtained findings convincingly demonstrated that the synthesized nanocomposite could be a composite with potential for multifunctional use.

Funding

The work proposed here does not received funds from any sources.

Availability of data and materials

The datasets or analyzed during the current study are available from the corresponding author on reasonable request.

CRediT authorship contribution statement

G. Sri balaji: Conceptualization, Material preparation, Data collection, Data analysis, Writing – original draft. S.Satheeskumar : Conceptualization, Supervision, Writing – review & editing, Validation.

Declaration of Competing Interest

The authors affirm that they have no known financial or interpersonal conflicts that would have seemed to have an impact on the research presented in this study. Data availability Data will be made available on request.

Acknowledgement

The author thanks the Department of Nanoscience and Technology,K.S. Rangasamy College of Technology (Autonomous), Tiruchengode, Tamil Nadu, India, for providing the resources necessary to carry out this research.

References.

1. D.J . Alderman Ministry of Agriculture, Fisheries and Food, Directorate of Fisheries Research, Fish Diseases Laboratory, Weymouth, England,: A review: Malachite green,: Journat of Fish Diseases ,8,289-29 (1985).
2. Berberidou, C., Poulios, I., Xekoukoulotakis, N.P., Mantzavinos, D. : Sonolytic, photocatalytic and sonophotocatalytic degradation of malachite green in aqueous solutions,: Applied Catalysis B: Environmental 74 (2007).
3. Franklin D. Lowy, M.D.: Staphylococcus aureus infections N Engl J Med ; 339:520-532 (1998).
4. Kaper, J., Nataro, J. & Mobley,: H. Pathogenic Escherichia coli.: Nat Rev Microbiol 2,: 123–140 (2004).
5. Rastogi A, Zivcak M, Sytar O, Kalaji HM, He X, Mbarki S AND Brestic M.: Impact of Metal and Metal Oxide Nanoparticles on Plant: A Critical Review. Front. Chem. 5:78 (2017).
6. Karli Gold, Buford Slay, Mark Knackstedt, Akhilesh K. Gaharwar.: Antimicrobial Activity of Metal and Metal-Oxide Based Nanoparticles,: Adv. Therap. (2018).
7. Nereyda niño-martínez, Marco felipe salas orozco, Gabriel-Alejandro Martínez-Castañón , Fernando torres Méndez AND Facundo Ruiz. Molecular Mechanisms of Bacterial Resistance to Metal and Metal Oxide Nanoparticles,Int. J. Mol. Sci., 20, 2808 (2019).
8. N.A. Travlou, D.A. Ginnakoudakis, M. Algarra, A.M. Labella, E. Rodríguezcastellón, T.J. Bandosz. S- and N-doped carbon quantum dots: Surface chemistry dependent antibacterial activity, Carbon (2018).
9. R.S. Kate, S.A. Khalate, R.J. Deokate. Overview of nanostructured metal oxides and pure nickel oxide (NiO) electrodes for supercapacitors: A review, Journal of Alloys and Compounds (2017).
10. Nibedita Behera, Manoranjan Arakha, Mamali Priyadarshinee, Biraja S. Pattanayak, Siba Soren, Suman Jha and Bairagi C. Mallick. Oxidative stress generated at nickel oxide nanoparticle interface results in bacterial membrane damage leading to cell dead,: RSC Adv., 9, 24888 (2019).
11. Michael Walker & David Parsons,. The biological fate of silver ions following the use of silver-containing wound care products,: a review-International Wound Journal., ISSN 1742-4801 (2012).
12. Loghman Karimi , Salar Zohoori , Mohammad Esmail Yazdanshenas. Photocatalytic degradation of azo dyes in aqueous solutions under UV irradiation using nano-strontium titanate as the nanophotocatalyst Journal of Saudi Chemical Society, pp.1319-6103 (2011).
13. M. Mohammadijooa, Z. Naderi khorshidia, S.K. Sadrnezhaad AND V. Mazinani. Synthesis and characterization of nickel oxide nanoparticle with wide band gap energy prepared via thermochemical processing,Nanoscience and Nanotechnology: An International Journal ;(1): 6-9,ISSN: 2278-1374(2014).
14. Shu juan Z, Jing. F, Jing .W AND Chang qing Z. One-step hydrothermal synthesis of silver-doped carbon quantum dots for highly selective detection of uric acid, Methods Appl. Fluoresc (2019).
15. Chang eun K , Pyung M, Sungyeon K, Jae-min M , Hyeon woo J, Jungsik Bang , Ilgu Yun. Effect of carrier concentration on optical bandgap shift in ZnO:Ga thin films,Thin Solid Films 518 6304–6307 (2010).
16. Cullis, A. G.; Canham. Visible light emission due to quantum size effect in highly porous crystalline silicon, L. T. Nature , 353, 335(1991).
17. Oday A. Hammadi, Mohammed K. khalaf, Firas J. Kadhim. Farbication of UV photodetector from nickel oxide nanoparticles deposited on silicon substrate by closedfield unbalanced dual magnetron sputtering techniques,Opt Quant Electron (2015).
18. Chanae Park , Juhwan K , Kangil L , Suhk kun O , Hee jae K, AND nam seok Park. Electronic, Optical and Electrical Properties of Nickel Oxide Thin Films Grown by RF Magnetron Sputtering,Applied Science and Convergence Technology Vol.24 No.3,, pp.72-76(2015).
19. Ashish chhaganlal Gandhi AND Sheng yun WU. Strong Deep-Level-Emission Photoluminescence in NiO Nanoparticles,Nanomaterials, 7, 231(2017).

20. S. Mohseni meybodi , S.A. Hosseini , M. Rezaee , S.K. Sadrnezhaad , D. Mohammadyani. Synthesis of wide band gap nanocrystalline NiO powder via a sonochemical method,ultrasonics Sonochemistry,19,841-845(2012).
21. Jan Poppe, Stephen G. Hickey, AND Alexander Eychmüller . Photoelectrochemical Investigations of Semiconductor Nanoparticles and Their Application to Solar Cells, J. Phys. Chem (2014).
22. A. P. Alivisatos. Perspectives on the Physical Chemistry of Semiconductor Nanocrystals,J. Phys. Chem, 100, 13226-13239(1996).
23. R. Anithadevi, C. Ravichandran. enhanced photo-degradation activity of hybrid ZnMgTiO2 nanocomposites against methyl orange dye under uv irradiation, Journal of Ovonic Research, p. 449 - 457 (2018).
24. Neelabh Srivastava and P C Srivastava. Realizing NiO nanocrystals from a simple chemical method,Bull. Mater. Sci., pp. 653–656(2010).
25. Subhash Dharmraj Khairnar AND Vinod shankar Shrivastava. Facile synthesis of nickel oxide nanoparticles for the degradation of Methylene blue and Rhodamine B dye: a comparative study,JOURNAL OF TAIBAH UNIVERSITY FOR SCIENCE, 1108–111(2019).
26. Fazal ur Rehman, Rashid Mahmood, Manel ben .A, Amor Hedfi, Amine Mezni , Sirajul Haq, Salah ud Din and Rimsha Ehsan. Physicochemical, Photocatalytic, Antibacterial, and Antioxidant Screening of Bergenia Ciliata Mediated Nickel Oxide Nanoparticles,Crystals, 11, 1137(2021).
27. Mohammed Baalousha, William How, Eugenia valsami-Jones and Jamie R. Lead. Overview of Environmental Nanoscience,Frontiers of Nanoscience,Vol. 7.(2014).
28. D. Mohammadyani, S.A. Hosseini and S.K. Sadrnezhaad. characterization of nickel oxide nanoparticles synthesized via rapid microwave-assisted route,International Journal of Modern Physics: Conference Series Vol. 5 270–276(2012).
29. Quanlong Xu, Liuyang Zhang, Bei Cheng, Jiajie Fan AND Jiaguo Yu. S-Scheme Heterojunction Photocatalyst,Chem 6, 1–17 (2020) .
30. Hamza A, Fatuase J.T., Waziri, S. M. and ajayi, O. A. Solar photocatalytic degradation of phenol using nanosized ZnO and α-e2O3,Journal of Chemical Engineering and Materials Science,Vol. 4(7), pp. 87-92 (2013).
31. Rekha Pachaiappan, Saravanan Rajendran, Pau Loke Show, Kovendhan Manavalan, Mu. Naushad. Metal/metal oxide nanocomposites for bactericidal effect: A review,Chemosphere,pp,0045-6535(2020).
32. James M. Slauch. How does the oxidative burst of macrophages kill bacteria? Still an open question,Molecular Microbiology, 80(3), 580–583 (2011).
33. Xiuli Dong, Weixiong Liang, Mohammed J. Meziani, Ya-ping Sun, and Liju Yang. Carbon Dots as Potent Antimicrobial Agents,Theranostics.; 10(2): 671–686(2020).
34. Baikun Li, Bruce E. Logan. Bacterial adhesion to glass and metal-oxide surfaces, Colloids and Surfaces B: Biointerfaces 36 ,81–90(2004) .
35. Ghazaleh Ilbeigi, Ashraf Kariminik, Mohammad Hasan Moshafi. The Antibacterial Activities of NiO Nanoparticles Against Some Gram-Positive and Gram-Negative Bacterial Strains,*Int J Basic Sci Med, 4(2):69-74* (2019)